

width decreases with increasing path length. A numerical model<sup>17</sup> for one relativistic plasma maser indicates a bandwidth that decreases to 20% for a brightness temperature of  $10^{20}$  K. Thus, for masers, high brightness tends to be incompatible with broad bandwidth.

Emission in strong plasma turbulence is associated with the nonlinear localization of electrostatic wave energy in the plasma source region, and the subsequent explosive collapse of wave packets that takes place over a few wave oscillation periods<sup>25,26</sup>. Numerical modelling<sup>27</sup> of individual pulses produced by strong plasma turbulence at 5 GHz predicts nanosecond radio bursts, and quasi-periodic structure due to resonant coupling between the plasma and radiative modes on the timescale of 1–3 ns, in agreement with our observations. Plasma turbulence is the only pulsar emission model for which a mechanism has been identified that can produce such extremely short giant radio pulses. We conclude, therefore, that giant pulse radio emission from the Crab pulsar results from the conversion of electrostatic turbulence in the pulsar magnetosphere by the mechanism of spatial collapse of nonlinear wavepackets.

The nanopulses we have detected represent an example of highly efficient coherent radio emission from a relativistic flow that serves as a prototype for coherent, transient radio emission from perhaps a larger class of sources, such as active galactic nuclei. Although extraordinary attention has been given to transients in X-ray<sup>28</sup> and gamma-ray wavelengths, radio transients represent a largely unexplored observational regime<sup>29</sup>. Indeed, the techniques we apply to recover the Crab giant pulses will be useful in the search for extrasolar radio bursts and pulsars in other galaxies. □

Received 8 July 2002; accepted 4 February 2003; doi:10.1038/nature01477.

1. Staelin, D. H. & Reifenstein, E. C. III Pulsating radio sources near the Crab nebula. *Science* **162**, 1481–1483 (1968).
2. Cognard, I., Shrauner, J. A., Taylor, J. H. & Thorsett, S. E. Giant radio pulses from a millisecond pulsar. *Astrophys. J.* **457**, L81–L84 (1996).
3. Romani, R. W. & Johnston, S. Giant pulses from the millisecond pulsar B1821–24. *Astrophys. J.* **557**, L93–L96 (2001).
4. Hankins, T. H. Microsecond intensity variations in the radio emissions from CP 0950. *Astrophys. J.* **169**, 487–491 (1971).
5. Hankins, T. H. & Rickett, B. J. Pulsar signal processing. *Meth. Comp. Phys.* **14**, 55–129 (Academic, New York, 1975).
6. Sallmen, S., Backer, D. C., Hankins, T. H., Moffett, D. & Lundgren, S. Simultaneous dual-frequency observations of giant pulses from the Crab pulsar. *Astrophys. J.* **517**, 460–471 (1999).
7. Lundgren, S. C. *et al.* Giant pulses from the Crab pulsar: A joint radio and gamma-ray study. *Astrophys. J.* **453**, 433–446 (1995).
8. Rickett, B. J. Amplitude-modulated noise: An empirical model for the radio radiation received from pulsars. *Astrophys. J.* **197**, 185–191 (1975).
9. Cordes, J. M. Pulsar radiation as polarized shot noise. *Astrophys. J.* **210**, 780–791 (1976).
10. Goldreich, P. & Julian, W. H. Pulsar electrodynamics. *Astrophys. J.* **157**, 869–880 (1969).
11. Rickett, B. J. & Cordes, J. M. In *Pulsars, IAU Symp. 95* (eds Sieber, W. & Wielebinski, R.) 107–109 (Reidel, Boston, 1981).
12. Popov, M. V. *et al.* Microstructure of pulsar radio pulses measured with a time resolution of 62.5 ns at 1650 MHz. *Astron. Rep.* **46**, 206–213 (2002).
13. Arendt, P. N. Jr & Eilek, J. A. Pair creation in the pulsar magnetosphere. *Astrophys. J.* **581** (in the press).
14. Buschauer, R. & Benford, G. General theory of coherent curvature radiation. *Mon. Not. R. Astron. Soc.* **177**, 109–136 (1976).
15. Asseo, E., Pelletier, G. & Sol, H. A non-linear radio pulsar emission mechanism. *Mon. Not. R. Astron. Soc.* **247**, 529–548 (1990).
16. Weatherall, J. C. Modulational instability, mode conversion, and radio emission in the magnetized pair plasma of pulsars. *Astrophys. J.* **483**, 402–413 (1997).
17. Lyutikov, M., Blandford, R. D. & Machabeli, G. On the nature of pulsar radio emission. *Mon. Not. R. Astron. Soc.* **305**, 338–352 (1999).
18. Weatherall, J. C. A relativistic-plasma Compton maser. *Astrophys. J.* **559**, 196–200 (2001).
19. Jenet, F. A., Anderson, S. B. & Prince, T. A. The first detection of coherent emission from radio pulsars. *Astrophys. J.* **558**, 302–308 (2001).
20. Cairns, I. H., Johnston, S. & Das, P. Intrinsic variability of the Vela pulsar: Lognormal statistics and theoretical implications. *Astrophys. J.* **563**, L65–L68 (2001).
21. Delaney, T. & Weatherall, J. C. Model for deterministic chaos in pulsar radio signals and search for attractors in the Crab and Vela pulsars. *Astrophys. J.* **519**, 291–302 (1999).
22. Benford, G. Model for the microstructure emission of pulsars. *Mon. Not. R. Astron. Soc.* **179**, 311–315 (1977).
23. Elitzur, M. *Astronomical Masers* 68–71 (Kluwer, Boston, 1992).
24. Moran, J. M. Statistical properties of the radiation fields from H<sub>2</sub>O masers. *Bull. Am. Astron. Soc.* **13**, 508 (1981).
25. Zakharov, V. E. Collapse of Langmuir waves. *Sov. Phys. JETP* **35**, 908–914 (1972).
26. Goldman, M. V. Strong turbulence of plasma waves. *Rev. Mod. Phys.* **56**, 709–735 (1984).

27. Weatherall, J. C. Pulsar radio emission by conversion of plasma wave turbulence: Nanosecond time structure. *Astrophys. J.* **506**, 341–346 (1998).
28. Strohmayer, T. E., Swank, J. H. & Zhang, W. in *The Active X-ray Sky: Results from BeppoSAX and RXTE* (eds Scarsi, L., Bradt, H., Giommi, P. & Fiore, F.) *Nucl. Phys. B (Proc. Suppl.)* **69**, 129 (1997).
29. Mészáros, P. Gamma-ray bursts: Accumulating afterglow implications, progenitor clues, and prospects. *Science* **291**, 79–84 (2001).

**Acknowledgements** T.H.H. thanks NRAO and NAIC for partial sabbatical leave support at the Green Bank and Arecibo Observatories. J.S.K. thanks NRAO for pre-doctoral support. We thank B. Driggers of TMS and LeCroy for the loan of a LeCroy LT584L oscilloscope, J. Ford at NRAO Green Bank for square-law detectors, NRAO Socorro for computer support and technical assistance, and the NSF for a research grant. The Arecibo Observatory is operated by Cornell University under a cooperative agreement with the National Science Foundation.

**Competing interests statement** The authors declare that they have no competing financial interests.

**Correspondence** and requests for materials should be addressed to T.H.H. (e-mail: thankins@aoc.nrao.edu).

.....

## An extended upper atmosphere around the extrasolar planet HD209458b

A. Vidal-Madjar\*, A. Lecavelier des Etangs\*, J.-M. Désert\*, G. E. Ballester†, R. Ferlet\*, G. Hébrard\* & M. Mayor‡

\* Institut d'Astrophysique de Paris, CNRS/UPMC, 98bis boulevard Arago, F-75014 Paris, France

† Lunar and Planetary Laboratory, University of Arizona, 1040 E. 4th St., Rm 901, Tucson, Arizona 85721-0077, USA

‡ Observatoire de Genève, CH-1290 Sauverny, Switzerland

The planet in the system HD209458 is the first one for which repeated transits across the stellar disk have been observed<sup>1,2</sup>. Together with radial velocity measurements<sup>3</sup>, this has led to a determination of the planet's radius and mass, confirming it to be a gas giant. But despite numerous searches for an atmospheric signature<sup>4–6</sup>, only the dense lower atmosphere of HD209458b has been observed, through the detection of neutral sodium absorption<sup>7</sup>. Here we report the detection of atomic hydrogen absorption in the stellar Lyman  $\alpha$  line during three transits of HD209458b. An absorption of  $15 \pm 4\%$  ( $1\sigma$ ) is observed. Comparison with models shows that this absorption should take place beyond the Roche limit and therefore can be understood in terms of escaping hydrogen atoms.

Far more abundant than any other species, hydrogen is well-suited for searching weak atmospheric absorptions during the transit of an extrasolar giant planet in front of its parent star, in particular over the strong resonant stellar ultraviolet Lyman  $\alpha$  emission line at 1,215.67 Å. Depending upon the characteristics of the planet's upper atmosphere, an H I signature much larger than that for Na I at 0.02% (ref. 7) is foreseeable. Three transits of HD209458b (named A, B and C hereafter) were sampled in 2001 (on 7–8 September, 14–15 September and 20 October, respectively) with the Space Telescope Imaging Spectrograph (STIS) onboard the Hubble Space Telescope (HST); the data set is now public in the HST archive. To partially overcome contamination from the Earth's Lyman  $\alpha$  geocoronal emission, we used the G140M grating with the  $52'' \times 0.1''$  slit (medium spectral resolution:  $\sim 20 \text{ km s}^{-1}$ ). For each transit, three consecutive HST orbits (named 1, 2 and 3 hereafter) were scheduled such that the first orbit (1,780 s exposure) ended before the first contact to serve as a reference, and the two following

ones (2,100 s exposures each) were partly or entirely within the transit.

The observed Lyman  $\alpha$  spectrum of HD209458 is typical for a solar-type star, with a double-peaked emission originating from the stellar chromosphere (Fig. 1). It also shows a wide central absorption feature due to neutral hydrogen in the interstellar medium. The geocoronal emission filled the aperture of the spectrograph, resulting in an extended emission line perpendicular to the dispersion direction. The extent of this emission along the slit allowed us to remove it at the position of the target star. We evaluated its variation both along the slit and from one exposure to another, and excluded the wavelength domain where the corresponding standard deviation per pixel is larger than 20% of the final spectrum. We concluded that the geocoronal contamination can be removed with high enough accuracy outside the central region ( $1,215.5 \text{ \AA} < \lambda < 1,215.8 \text{ \AA}$ , labelled 'Geo' in Figs 2, 4).

From the two-dimensional (2D) images of the far-ultraviolet (FUV) multi-anode microchannel array (MAMA) detector, the STIS standard pipeline extracts one-dimensional spectra in which the dark background has not been removed. The background level was systematically increasing from one exposure to the next within each of the three visits, but still remained below 2% of the peak intensity of the stellar signal. We therefore reprocessed the 2D images by using two independent approaches. The first one uses the 2D images provided by the standard pipeline and interpolates the background (including the Earth's geocoronal emission) with a polynomial fitted per column above and below the spectrum region. The second method starts from the 2D raw images to which is applied a dark background correction from a super-dark image (created for the period of the observations) as well as a subtraction of the geocoronal emission measured along the slit, away from the stellar spectrum. The differences between the results of both approaches are negligible, showing that systematic errors generated through the background corrections are small compared to the statistical errors. Those errors are dominated by photon counting

noise to which we added quadratically the error evaluated for both the dark background and geocoronal subtractions.

The Lyman  $\alpha$  line profiles observed before and during the transits are plotted in Fig. 2. The three exposures outside the transits (exposures A1, B1 and C1) and the three entirely within the transits (A2, B3 and C3) were co-added to improve the signal-to-noise ratio. An obvious signature in absorption is detected during the transits, mainly over the blue side of the line, and possibly at the top of the red peak.

To characterize this signature better, we have defined two spectral domains: 'In' and 'Out' of the absorption. The In domain is a wavelength interval limited by two variables  $\lambda_1$  and  $\lambda_2$  (excluding the Geo geocoronal region). The Out domain is the remaining wavelength coverage within the interval 1,214.4–1,216.8  $\text{\AA}$ , for which the Lyman  $\alpha$  line intensity can be accurately measured at the time of the observation. The corresponding In/Out flux ratio derived for each exposure is shown in Fig. 3, revealing the absorption occurring during the transits. To evaluate whether this detection is sensitive to a particular choice of  $\lambda_1$  and  $\lambda_2$ , we averaged the three ratios before the transits and the three ratios entirely within the transits. We calculated the averaged pre-transits over mid-transits ratio as a function of  $\lambda_1$  and  $\lambda_2$  and propagated the errors through boot-strap estimations of the ratio calculated with 10,000 randomly generated spectra according to the evaluated errors over each individual pixel (Fig. 2c). The averaged ratio is always significantly below 1, with the minimum at  $\lambda_1 = 1,215.15 \text{ \AA}$  and  $\lambda_2 = 1,216.1 \text{ \AA}$ . In the interval defined by these two wavelengths, the Lyman  $\alpha$  line is reduced by  $15 \pm 4\%$  ( $1\sigma$ ) during the transit. This is a larger-than- $3\sigma$  detection of an absorption in the hydrogen line profile during the planetary transits.

HD209458 (G0V) is close to solar type, for which time variations are known to occur in the chromospheric Lyman  $\alpha$  line<sup>8</sup>. We thus evaluated the In/Out ratio in the solar Lyman  $\alpha$  line profile as measured over the whole solar disk by the Solar Ultraviolet Measurements of Emitted Radiation (SUMER) instrument onboard

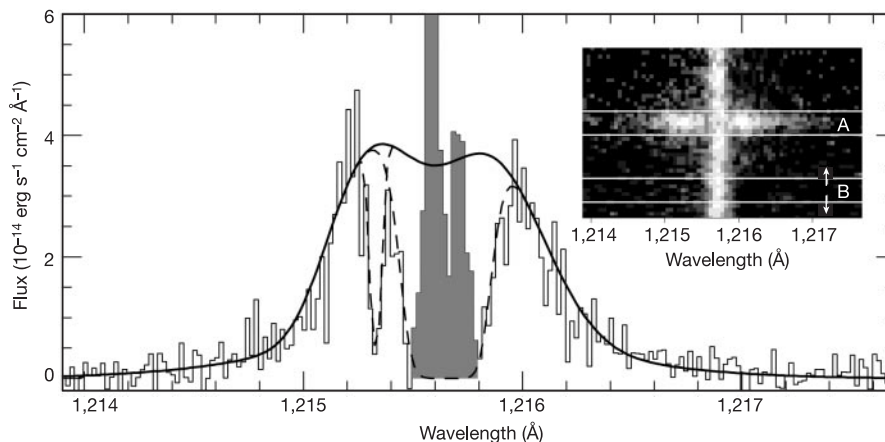


**Figure 1** The HD209458 Lyman  $\alpha$  emission line. This high-resolution spectrum (histogram) was obtained with the E140M echelle grating and the  $0.2'' \times 0.2''$  wide slit with a spectral resolution of  $5 \text{ km s}^{-1}$ ; it was not used in the present analysis, but it allows the different components of the line profile to be seen. The continuum is a double-peaked emission line originating from the stellar chromosphere: the temperature increase in the lower chromosphere causes an emission line with a central dip due to the high opacity of the abundant hydrogen atoms (solid line). The observed spectrum also has a narrow absorption line (1,215.3  $\text{\AA}$ , barely seen at lower resolution) and a central wide absorption line (1,215.6  $\text{\AA}$ ) due to the interstellar deuterium and hydrogen, respectively (dashed lines). The grey zone represents the fraction of the spectrum contaminated by the geocoronal emission, which is double-peaked in that case because the plotted spectrum

is the average of four exposures obtained at two different epochs. The inset shows a small portion of the 2D image of a G140M first-order spectrum containing the stellar Lyman  $\alpha$  profile and a sample of the geocoronal signal. This spectrum is one of the nine spectra used for this analysis. The G140M spectra have lower spectral resolution but higher signal-to-noise ratio. The stellar spectrum is seen as a horizontal line where the two peaks are resolved from the geocoronal emission (vertical line along the slit). The one-dimensional spectra are obtained by vertically adding around ten pixels within the A band. Measurements along the slit direction ( $\sim 800$  pixels available), for example at the position of the B band, allow us to estimate the geocoronal contamination and the background subtraction as well as the corresponding uncertainties.

the Solar and Heliospheric Observatory (SOHO)<sup>9</sup> during the last solar cycle from 1996 to 2001, that is, from quiet to active Sun. During this time, the total solar Lyman  $\alpha$  flux varies by about a factor of two, while its In/Out ratio varies by less than  $\pm 6\%$ . Within a few months, a time comparable to our HD209458 observations, the solar In/Out ratio varies by less than  $\pm 4\%$ . This is an indication that the absorption detected is not of stellar origin but is due to a transient absorption occurring during the planetary transits.

A bright hot spot on the stellar surface hidden during the planetary transit is also excluded. Such a hot spot would have to contribute about 15% of the Lyman  $\alpha$  flux over 1.5% of the stellar surface occulted by the planet, in contradiction with Lyman  $\alpha$  inhomogeneities observed on the Sun<sup>10</sup>. Furthermore, this spot would have to be perfectly aligned with the planet throughout the transit, at the same latitude as the Earth's direction, and with a peculiar narrow single-peaked profile confined over the In spectral region. It seems unlikely that a stellar spot could satisfy all these conditions.

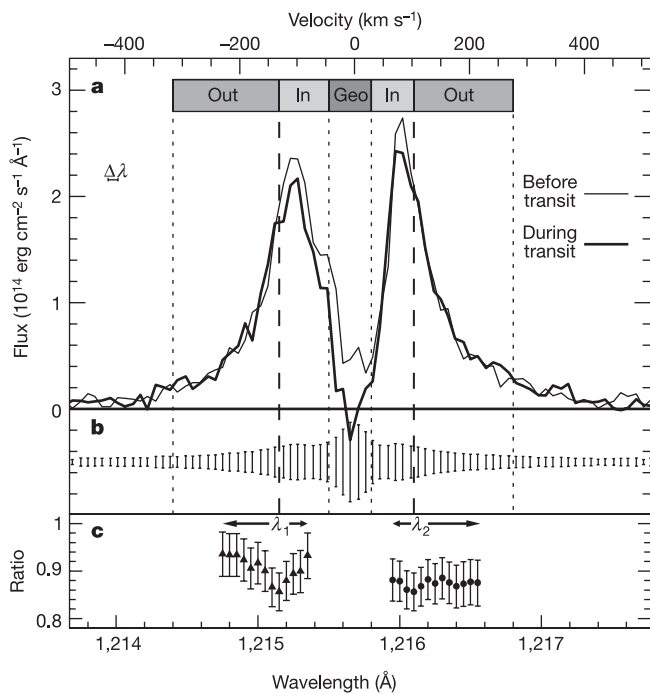


**Figure 2** The HD209458 Lyman  $\alpha$  profile observed with the G140M grating. The geocoronal emission has been subtracted; the propagated errors are consequently larger in the central part of the profile, particularly in the Geo domain (see text).  $\Delta\lambda$  represents the spectral resolution. **a**, The thin line shows the average of the three observations performed before the transits (exposures A1, B1 and C1); the thick line shows the average of the three observations recorded entirely within the transits (exposures A2, B3 and C3). Variations are seen in the In domain as absorption over the blue peak of the line and partially over the red peak (between  $-130 \text{ km s}^{-1}$  and  $100 \text{ km s}^{-1}$ ). Quoted velocities are in the stellar reference frame, centred on  $-13 \text{ km s}^{-1}$  in the heliocentric reference frame. **b**,  $\pm 1\sigma$  error bars. **c**, The ratio of the two spectra in the In domain, the spectra being normalized such that the ratio is 1 in the Out domain. This ratio is plotted as a function of  $\lambda_1$  using  $\lambda_2 = 1,216.10 \text{ \AA}$  (triangles), and as a function of  $\lambda_2$  using  $\lambda_1 = 1,215.15 \text{ \AA}$  (circles). The ratio is always significantly below 1, with a minimum at  $\lambda_1 = 1,215.15 \text{ \AA}$  ( $-130 \text{ km s}^{-1}$ ) and  $\lambda_2 = 1,216.10 \text{ \AA}$  ( $100 \text{ km s}^{-1}$ ). In the domain defined by these values, the Lyman  $\alpha$  intensity decreases during the transits by  $15 \pm 4\%$ . The detection does not strongly depend on a particular selection of the domain. While the decrease of the Lyman  $\alpha$  intensity is not sensitive to the position of  $\lambda_2$ , it is more sensitive to the position of  $\lambda_1$ , showing that most of the absorption occurs in the blue part of the line. Using the whole domain where the absorption is detected, the exoplanetary atmospheric hydrogen is detected at more than  $3\sigma$ .

Finally, we confirmed with various tests that there are no correlations between the geocoronal variations and the detected signature in absorption. One method is presented in Fig. 4, showing that a contamination of the In domain by the geocorona is excluded. We thus conclude that the detected profile variation can only be related to an absorption produced by the planetary environment.

The observed 15% intensity drop is larger than expected *a priori* for an atmosphere of a planet occulting only 1.5% of the star. Although the small distance (8.5 stellar radii) between the planet and the star results in an extended Roche lobe<sup>11</sup> with a limit at about 2.7 planetary radii (that is, 3.6 Jupiter radii), the filling up of this lobe gives a maximum absorption of about 10% during the planetary transit. Because a more important absorption is detected, hydrogen atoms must cover a larger area: a drop of 15% corresponds to an occultation by an object of 4.3 Jupiter radii. This is clearly beyond the Roche limit as theoretically predicted<sup>6</sup>. Thus some hydrogen atoms should escape from the planet. The spectral absorption width shows independently that the atoms have large velocities relative to the planet. Thus hydrogen atoms must be escaping the planetary atmosphere.

We have built a particle simulation in which we assumed that hydrogen atoms are sensitive to the stellar radiation pressure

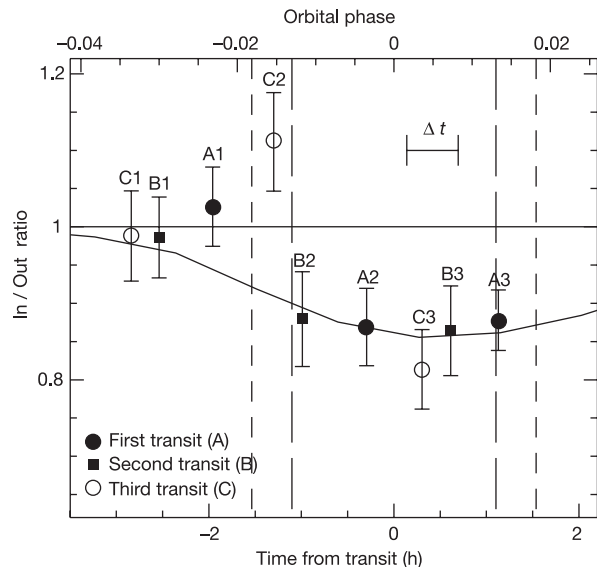


**Figure 3** Relative flux of Lyman  $\alpha$  as a function of the HD209458's system phase. The averaged ratio of the flux is measured in the In ( $1,215.15\text{--}1,215.50 \text{ \AA}$  and  $1,215.80\text{--}1,216.10 \text{ \AA}$ ) and the Out ( $1,214.40\text{--}1,215.15 \text{ \AA}$  and  $1,216.10\text{--}1,216.80 \text{ \AA}$ ) domains in individual exposures of the three observed transits of HD209458b. The central time of each exposure is plotted relative to the transit time. The vertical dashed lines indicate the first and the second contact at the beginning and the end of the transit; the exposures A1, B1 and C1 were performed before the transits, and the exposures A2, B3 and C3 were entirely within the transits. The ratio is normalized to the average value of the three observations completed before the beginning of the transits. The  $\pm 1\sigma$  error bars are statistical; they are computed through boot-strap estimations (see text). The In/Out ratio smoothly decreases by around 15% during the transit. The thick line represents the absorption ratio modelled through a particle simulation which includes hydrogen atoms escaping from the planet. In this simulation, hydrogen atoms are sensitive to the radiation pressure above an altitude of 0.5 times the Roche radius, where the density is assumed to be  $2 \times 10^5 \text{ cm}^{-3}$ ; these two parameters correspond to an escape flux of  $\sim 10^{10} \text{ g s}^{-1}$ . The stellar radiation pressure is taken to be 0.7 times the stellar gravitation. The mean lifetime of escaping hydrogen atoms is taken to be 4 h. The model yields an atom population in a curved comet-like tail, explaining why the computed absorption lasts well after the end of the transit.

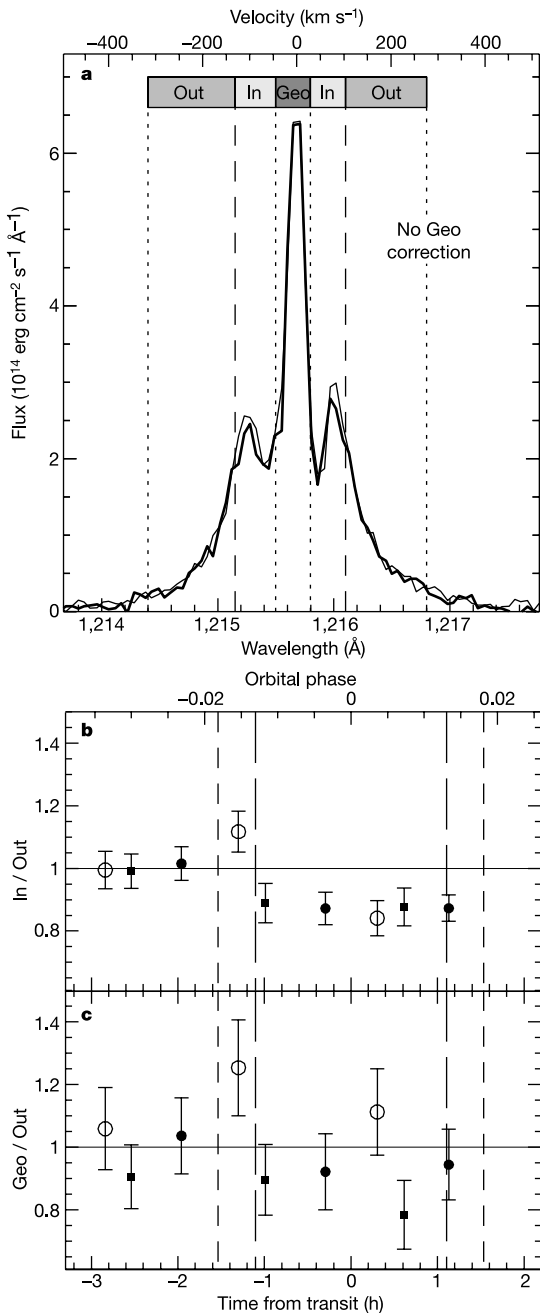


**Figure 4** Spectra and ratios with no geocoronal correction. To investigate the possibility that a bad estimate of the geocoronal correction may cause the detected signal, the spectra and ratios are plotted without this correction. First, note that the geocoronal emission is of the order of the stellar flux, and its peak value is never larger than three times the stellar one. Consequently, the correction is very small outside the Geo domain. **b** shows the same evaluation of the In/Out ratios as made in Fig. 3, with no geocoronal and no background correction. It appears that the impact of the geocoronal correction on these ratios is negligible. To further show that the ‘wings’ of the geocoronal emission do not carry the detected transit signal, **c** shows the Geo/Out ratios, where Geo is the total flux due to the geocorona. If the flux in the In domain was significantly affected by the geocorona, the Geo/Out ratios should present a signal similar to the In/Out ratios plotted in Fig. 3. The Geo/Out ratios are found to be random fluctuations around the average of the A1, B1 and C1 values. There is no consistent signature of the transit in the geocoronal variations. As in Fig. 2a, **a** shows the average of the three spectra obtained before and during the transits (thin and thick lines, respectively). Quoted velocities are in the stellar reference frame. Here the spectra are without any geocoronal correction. A simple constant has been subtracted to compensate for the mean background levels in order to have matching spectra in the Out domain. This clearly shows that the absorption signature is present even without the geocoronal correction.

inside and outside the Roche lobe. Their motion is evaluated by taking into account both the planetary and stellar gravities. The Lyman  $\alpha$  radiation pressure is known to be 0.7 times the stellar gravity, the escape flux and the neutral hydrogen lifetime being free parameters. The lifetime of hydrogen is limited to a few hours owing to stellar extreme ultraviolet ionization. Escaping hydrogen atoms expand in an asymmetric comet-like tail and progressively disappear when moving away from the planet. This simple scenario is consistent with the observations (Fig. 3). In this model, atoms in the evaporating coma and tail cover a large area of the star, and most are blueshifted because of the radiation pressure repelling them away from the star. The detection of most of the absorption in the blue part of the line is consistent with these escaping atoms. On the other hand, more observations are needed to clarify whether an absorption is also present in the red part of the line.

To account for the observed absorption depth, the particle simulation implies a minimum escape flux of around  $10^{10} \text{ g s}^{-1}$ . However, owing to saturation effects in the absorption line, a flux larger by several orders of magnitude would produce a similar absorption signature. So, to evaluate the actual escape flux, we need to estimate the vertical distribution of hydrogen atoms up to the Roche limit, in an atmosphere extended by the stellar tidal forces and heated by many possible mechanisms. These effects may lead to a much larger escape flux. A detailed calculation is beyond the scope of this Letter. This raises the question of the lifetime of evaporating extrasolar planets which may be comparable to the star’s lifetime itself. If so, the so-called ‘hot Jupiters’ could evolve faster than their parent star, eventually becoming smaller objects, which could look like ‘hot hydrogen-poor Neptune-mass’ planets. This evaporation process, more efficient for planets close to their star, might explain the very few detections<sup>12,13</sup> of ‘hot Jupiters’ with orbiting periods shorter than three days. □

Received 13 September 2002; accepted 27 January 2003; doi:10.1038/nature01448.

- Henry, G. W., Marcy, G. W., Butler, R. P. & Vogt, S. S. A transiting “51 Peg-like” planet. *Astrophys. J.* **529**, L41–L44 (2000).
- Charbonneau, D., Brown, T. M., Latham, D. W. & Mayor, M. Detection of planetary transits across a Sun-like star. *Astrophys. J.* **529**, L45–L48 (2000).
- Mazeh, T. *et al.* The spectroscopic orbit of the planetary companion transiting HD 209458. *Astrophys. J.* **532**, L55–L58 (2000).
- Bundy, K. A. & Marcy, G. W. A search for transit effects in spectra of 51 Pegasi and HD 209458. *Proc. Astron. Soc. Pacif.* **112**, 1421–1425 (2000).
- Rauer, H., Bockelée-Morvan, D., Coustenis, A., Guillot, T. & Schneider, J. Search for an exosphere around 51 Pegasi B with ISO. *Astron. Astrophys.* **355**, 573–580 (2000).
- Moutou, C. *et al.* Search for spectroscopical signatures of transiting HD 209458b’s exosphere. *Astron. Astrophys.* **371**, 260–266 (2001).
- Charbonneau, D., Brown, T. M., Noyes, R. W. & Gilliland, R. L. Detection of an extrasolar planet atmosphere. *Astrophys. J.* **568**, 377–384 (2002).
- Vidal-Madjar, A. Evolution of the solar Lyman alpha flux during four consecutive years. *Sol. Phys.* **40**, 69–86 (1975).
- Lemaire, P. *et al.* in *Proc. Symp. SOHO 11, From Solar Min to Max: Half a Solar Cycle with SOHO* (ed. Wilson, A.) 219–222 (ESA SP-508, ESA Publications Division, Noordwijk, 2002).
- Prinz, D. K. The spatial distribution of Lyman alpha on the Sun. *Astrophys. J.* **187**, 369–375 (1974).
- Paczynski, B. Evolutionary processes in close binary systems. *Annu. Rev. Astron. Astrophys.* **9**, 183–208 (1971).
- Cumming, A., Marcy, G. W., Butler, R. P. & Vogt, S. S. The statistics of extrasolar planets: Results from the Keck survey. Preprint astro-ph/0209199 available at (<http://xxx.lanl.gov>) (2002).
- Konacki, M., Torres, G., Jha, S. & Sasselov, D. D. An extrasolar planet that transits the disk of its parent star. *Nature* **421**, 507–509 (2003).

**Acknowledgements** This work is based on observations with the NASA/ESA Hubble Space Telescope, obtained at the Space Telescope Science Institute, which is operated by AURA, Inc. We thank M. Lemoine, L. Ben Jaffel, C. Emerich, P. D. Feldman and J. McConnell for comments, J. Herbert and W. Landsman for conversations on STIS data reduction, and J. Valenti for help in preparing the observations.

**Competing interests statement** The authors declare that they have no competing financial interests.

**Correspondence** and requests for materials should be addressed to A.V.-M. (e-mail: [alfred@iap.fr](mailto:alfred@iap.fr)).